technische universität
dortmund

Arbeit zur Erlangung des akademischen Grades
Bachelor of Science

Discrimination of Standard Model and EFT contributions in single top production with a photon

Cyrus Walther
geboren in Dortmund

2020

Lehrstuhl für Experimentelle Physik IV
Fakultät Physik
Technische Universität Dortmund

Erstgutachter:	Priv. Doz. Dr. Johannes Erdmann
Zweitgutachter:	Prof. Dr. Bernhard Spaan
Abgabedatum:	25. June 2020

Abstract

The single top quark production with a photon is an important test of the Standard Model in order to investigate the top quark characteristics regarding the electroweak interaction. Therefore, the impact of Effective Field Theories on the electroweak characteristics of the top quark is investigated, by explicating the dimension-six operators $\mathcal{O}_{tW}$ and $\mathcal{O}_{tW}$. The impact of Effective Field Theory operators on the cross section is discussed and its influence on kinematic variables related to the photon is investigated. Moreover, a neural network is applied to discriminate Effective Field Theory contributions as signal and Standard Model contributions as background. Besides, the Standard Model top quark pair production with a photon is considered as background as well. Two neural networks are trained separately for $\mathcal{O}_{tW}$ and $\mathcal{O}_{tW}$ contributions, whereas both neural networks show good discrimination of signal and background events.

Contents

1 Introduction

The Standard Model of particle physics (SM) describes the fundamental particles and their interactions with each other. It covers three of the four fundamental interactions and has been intensively researched to test its predictions and is not refuted to this day.

Still, there are several arguments, which lead to the fact that there are limitations of the SM of particle physics and there are other theoretical approaches which may explain phenomena that are beyond the scope of the SM (BSM). Effective Field Theory (EFT) can be used as a model independent approach to describe those phenomena, without assuming specific underlying mechanisms. EFT approaches consist of the central idea that new physics, which is not be included in the SM, becomes directly visible at higher energy scales than those we investigate in current experiments. Iit describes the impact of this new physics on the investigated energy scale by introducing multidimensional operators. These can change coupling strengths or allow for new vertices.

In this thesis, the EFT approach is chosen to investigate possible BSM contributions in single top quark production with a photon, which is referred to as $tq\gamma$. It is sensitive to the coupling of the top quark to the W boson as well as to the photon. Therefore, $tq\gamma$ is an important SM test for the electroweak coupling of the top quark. The $tq\gamma$ process has not been observerd yet, but an evidence for $tq\gamma$ was claimed by the CMS Collaboration in 2018 corresponding to 4.4 standard deviations [1]. With the inclusion of more data it may be feasible to observe this process in the near future and therefore, study its properties and hence also possible EFT contributions to analyze potential BSM effects. A first analysis of the sensitivity of dimension-six operators in $tq\gamma$ was performed in a bachelor thesis [2].

This bachelor thesis continues and expands the study by investigating the impact of EFT operators depending on the photon origin and aims for the discrimination of EFT and SM contributions. First the photon origin is investigated and interference effects are studied. Second the impact of EFT operators on the $tq\gamma$ cross section is examined for different photon origins. Third photon kinematics are analyzed with SM and EFT data to highlight and compare the EFT influence on kinematic properties to the SM. Finally MadGraph5_aMC NLO [3] samples are separately created for pure EFT terms and for interference terms of SM and EFT contributions. Those samples are used to discriminate the events with a neural network approach and to evaluate the potential of this approach.

2 Single top quark production with a photon in the Standard Model

This chapter describes the $tq\gamma$ process in the context of the SM. Firstly, the SM is briefly explicated. Secondly, the top quark production at LHC and its characteristics are introduced as well as the $tq\gamma$ process, as described in the SM. Finally, this Chapter concludes by highlighting the limitations of the SM.

2.1 A brief overview of the Standard Model

The SM is a quantum field theory based, gauge theory and describes three of the four fundamental interactions, namely the strong, the weak and the electromagnetic interaction. Many SM measurements have been done and none refutes the SM.

The SM consists of the particles shown in Figure 2.1. These particles can be grouped by their spin into two categories. The first group of particles have integer spin and are called bosons. Gauge bosons mediate the three fundamental interactions described by the SM. Each gauge boson couples to a different particle feature. Gluons are massless gauge bosons and mediate the strong interaction. They couple to color charged particles and carry color charge themselves. The massless photon mediates the electromagnetic interaction and couples to the electric charge. It neither carries electric nor a color charge. The Z_0 boson and the $W^{\pm}$ bosons mediate the weak interaction, all three are massive, where $W^{\pm}$ carry electric charge. The $W^{\pm}$ bosons couple to the weak isospin and only with left-handed chirality states of the particle. The Z_0 boson couples to the hypercharge, which combines information about electric charge and weak isospin.

The second group consists of particles with half-integer spin ($s = \frac{1}{2}, ...$). These particles are called fermions. The group of fermions can again be divided into two categories, namely leptons and quarks. Quarks as well as leptons can be subdivided into three generations, each consisting of two quarks and two leptons. The first and lightest of these generations consists namely of up and down quark, the electron and the electron neutrino. Up and down quarks and electrons constitute the building blocks of the stable matter. The other generations are assembled as shown in Figure 2.1 In comparison to leptons, quarks carry color charge. Therefore, gluons only interact with quarks and themselves. As the coupling strength of the strong interaction is not constant as a function of distance between the interacting particles, only bound states of quarks can be observed. This phenomenon is called confinement. Additionally, every fermion has a separate feature called flavor. All fermions except neutrinos interact with the photon due to their electric charge, of which up-type quarks carry $+\frac{2}{3}$ and down-type quarks carry $-\frac{1}{3}$. Besides $W^{\pm}$ are the only particles that can change particle flavor. The Z_0 boson interacts with all charged and/or

left-handed particles. Therefore, right-handed neutrinos do not interact with any fundamental interaction and they do not exist in the SM. Furthermore there is an antifermion with i.a. opposite electric charge for every presented fermion.

The Higgs mechanism solves the requirement of massless fermions and bosons in the SM by spontaneously breaking the electroweak symmetry. The fermions then become massive by interacting with the Higgs field and the bosons acquire their mass through the Higgs mechanism. The interaction of the scalar Higgs boson and the fermions is called Yukawa interaction. Before the electroweak symmetry breaking the gauge bosons are exist in electroweak eigenstates, namely W^1, W^2, W^3 and B. By rotation W^3 and B can be rewritten in mass eigenstate representation Z_0 and γ. By linear combination W^1 and W^2 can be rewritten as W^+ and W^-. This is shown in Equation 2.1-2.3.

$$Z = \cos(\theta_W)W^3 - \sin(\theta_W)B \tag{2.1}$$

$$\gamma = \sin(\theta_W)W^3 + \cos(\theta_W)B \tag{2.2}$$

$$W^{\pm} = \frac{1}{\sqrt{2}}(W^1 \pm iW^2) \tag{2.3}$$

Only the mass eigenstates can be observed. Due to 2.1-2.3, deductions from this observation can be drawn for the electroweak eigenstates.

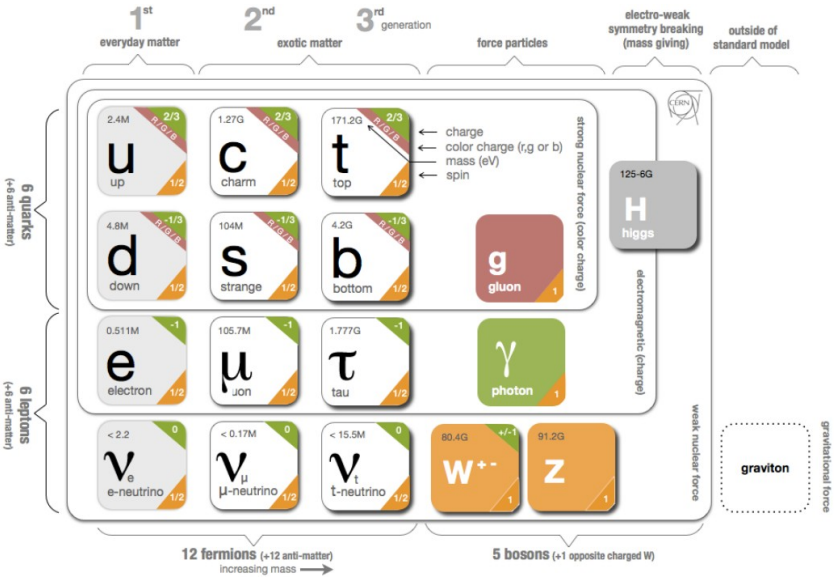

Figure 2.1: The particles of the SM summarized in their groups and labeled with their characteristic quantum numbers. Particles contributing to an interaction are assorted in corresponding boxes[4].

2.2 The $tq\gamma$ process in the Standard Model

The top quark is the up-type quark of the third generation. It is the heaviest quark with a mass of $m_t = 173.7 \pm 1.5(stat.) \pm 1.4(sys.)^{1.0}_{-0.5}(theo.)$ GeV [**tmass**]. Due to its electrical charge of $+\frac{2}{3}e$ it couples electromagnetically. It couples with gluons, as it has a color charge and it also couples weak with its weak isospin of $+\frac{1}{2}$. The top quarks decay width $\Gamma = 1.9 \pm 0.5$ GeV [5] is too short to build bound states, which leads to top quarks decaying right after their production. Therefore it is possible to draw conclusions from the decay products on the top quark.

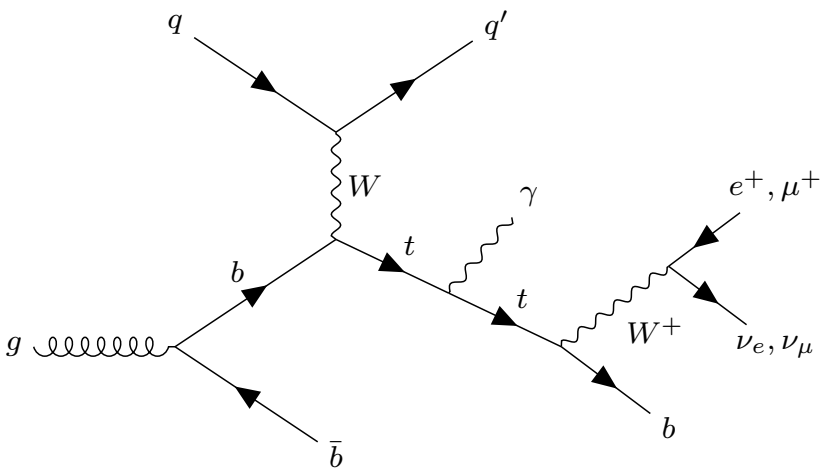

Figure 2.2: Leading order $tq\gamma$ production process feynman graph in the t-channel

Top quarks can be produced e.g. in proton proton collisions at the LHC [6]. Mainly top quarks can be produced in pairs or singly. The single top quark production is sensitive to the coupling of the top quark to the W boson and was discovered at the Tevatron in 2009 [7]. A bottom quark produced in pair production and an up type quark exchange a W boson. A single top quark and a down-type quark are produced and after a short time $\tau = \frac{1}{\Gamma}$ the top quark decays into a bottom quark and a W boson. The top quark is likely to decay into a bottom quark and a W boson because the transition probability of top and bottom quark is approximately ≈ 1. A photon can be radiated from any of the electrically charged particles in Figure 2.2, e.g. from the top quark. Thid process is referred to as $tq\gamma$. An Evidence for this process, corresponding to $\sigma = 4.4$, was found and a fiducial cross section of $\sigma(pp \to t\gamma j)(t \to \mu\nu b) = 115 \pm 17(stat) \pm 30(syst)$fb was measured in the phase space of $p_T^\gamma > 25$GeV and $\Delta R(\mu/j_b/j_{light}, \gamma) > 0.5$ by the CMS Collaboration [8].

2.3 Limitations of the Standard Model

As described in the previous sections, the SM is a frequently tested theory. Despite the measurements not refuting the SM there are different open questions, some of those are explained below.

First of all the baryon asymmetry describes the phenomenon that the number of baryons we observe in the universe is way higher than the number of antibaryons [9]. This huge difference cannot be explained by the SM.

Secondly, there are significant discrepancies between the observed matter and the matter we expect from different phenomena in the SM. An example for this are rotational curves of galaxies that do not match the gravitational profile we observe. This leads to the fact that in galaxies is more matter than we can observe [10]. Approximately 25% of the total matter is expected to exist in so-called dark matter.

Furthermore, we observe that neutrinos oscillate into different flavor states [11]. Therefore they are required to have mass. According to experiments the neutrino mass is too small to arise from a vacuum expectation value of the Higgs field [12] and SM expects the neutrinos to be massless. Currently experiments on this sector are running to investigate the neutrino mass, such as KATRIN [13].

Additionally, the strong interaction does not violate the CP-parity. In the theory of strong interaction a CP-violating phase is built-in and there is no explicit reason why it should be zero [14]. This is considered a conceptual puzzle of the SM and contradicts its instinctiveness.

Concluding the explicit facts, there is a strong evidence that the SM is not the final theory. Hence, it has to be expanded to explain further problems.

3 The top-γ vertex in the context of Effective Field Theory

This chapter gives a brief overview of EFT. Moreover, it depicts the dimension-six operator approach and its aspects applying to the $t\gamma$ vertex.

3.1 Introduction to Effective Field Theory

The idea of Effective Field Theories is to describe the impact of superordinate mechanisms that directly manifest at the energy scale $\mathcal{E}$ for energy scales $\mathcal{E}' \ll \mathcal{E}$.

The Fermi theory also known as the four-fermion interaction is one example of EFTs. It describes the decay of a neutron into a proton, an electron and an electron-$\bar{\nu}$, referred to as β-decay. Today it is known that this process is the transition of a down quark into an up quark by emitting a W boson that decays into an electron and an electron-$\bar{\nu}$. As the W boson is massive, the process is suppressed for energy scales $\mathcal{E}' \ll \mathcal{E}$ with $\mathcal{E} = m_W = (80.370 \pm 0.019)$ GeV[15]. Since the transfered momentum that arises in β-decay is $q = \mathcal{E}' \approx 1$ MeV the process is suppressed. Equation 3.1 illustrates that at energy scales $q \ll m_W$ the Fermi coupling approximates the weak coupling well, with α_{Weak} as the weak coupling constant and q the transfered momentum the W boson receives from the down quark.

$$\frac{\alpha_{Weak^2}}{q^2 - m_W^2} \overset{q \ll m_W}{\approx} \frac{\alpha_{Weak}^2}{m_W^2} \approx G_F \approx 1.166 \times 10^{-5} \ \text{GeV}^{-2}[16] \tag{3.1}$$

At the time, Fermi used a bottom up approach since the underlying mechanism was not known [17]. He treated this phenomenon as a point-like interaction with a definite coupling strength G_F 3.1. Since his EFT approach suits very well for observations on the $E' \ll E = m_W$ energy scale, this phenomenon and other can still be described by the Fermi theory.

EFT approaches introduce multidimensional effective field operators $\mathcal{O}$ into the present formalisms. These operators can modify or create vertices that expand the SM. The operators have a mass dimension, generally introduced as $\mathcal{D}$ and a corresponding coupling strength c_i, named Wilson coefficient. To introduce the operators to the SM, the Lagrangian density function $\mathcal{L}_{SM}$ is expanded by $\mathcal{L}_{EFT}$. In order to combine $\mathcal{L}_{SM}$ and $\mathcal{L}_{EFT}$ the mass dimensions of both Lagrangians have to equal. Since the EFT Lagrangian is defined by the multidimensional operators, it is necessary to adjust the mass dimension of the operators. Therefore the operators are divided by the energy scale exponentiated by $\mathcal{D} - 4$, because the SM is characterized

by $\mathcal{D}_{SM} = 4$. The Equation 3.2 defines the EFT Lagrangian, with its energy scale $\mathcal{E}$.

$$\mathcal{L}_{EFT} = \sum_i \frac{c_i}{\mathcal{E}^{\mathcal{D}_i - 4}} \mathcal{O}_i^{(\mathcal{D})} \tag{3.2}$$

This thesis considers only one dimension-six operator at a time, which leads to the Lagrangian density illustrated in equation 3.3.

$$\mathcal{L} = \mathcal{L}_{SM} + \frac{c}{\mathcal{E}^2} \mathcal{O} \tag{3.3}$$

The total cross section σ_{tot} can be derived from Equation 3.3 and is given in Equation 3.4, with $C = \frac{c}{\mathcal{E}^2}$. Herein σ_{SM} is the SM cross section, σ_{INT} is the interference terms of SM and EFT contributions and σ_{EFT} is the EFT cross section.

$$\sigma_{tot} = \sigma_{SM} + \sigma_{INT} C + \sigma_{EFT} C^2. \tag{3.4}$$

3.2 Dimension-six operators impacting the top-γ vertex

The general EFT approach can be applied measurements of the top quark. The vertex under study in the $tq\gamma$ process is the emission of the photon by the top quark, which is referred to as $t\gamma$. The two effective field operators given in Equation 3.5 and Equation 3.6 affect the $t\gamma$ vertex and the operator in 3.6 also affects the tW vertex[**O**].

$$\mathcal{O}_{tB} = (\bar{q}_3 \sigma^{\mu\nu} t_R) \tilde{\phi} B_{\mu\nu} \tag{3.5}$$

$$\mathcal{O}_{tW}^I = (\bar{q}_3 \sigma^{\mu\nu} \tau^I t_R) \tilde{\phi} W_{\mu\nu}^I \tag{3.6}$$

The compounds in this equation are defined as:

- t_R represents the right handed top quark
- $\bar{q}_3$ represents the left handed quark doublet of the third generation
- τ^I are the Pauli matrices
- $\sigma^{\mu\nu} = \frac{i}{2}[\gamma^\mu, \gamma^\nu]$, where γ^ν are the Dirac matrices.
- $\tilde{\phi}$ is the complex conjugated Higgs doublet multiplied with the antisymmetric SU(2) tensor

- $B_{\mu\nu}$ $W^I_{\mu\nu}$ are the fields of the electroweak eigenstates B, W^1, W^2 and W^3

Since the fields of the electroweak eigenstates are named $B_{\mu\nu}$ and $W^I_{\mu\nu}$, the corresponding rescaled Wilson coefficients can be referred to as C_{tB} and C_{tW}.

The effective field operators have specific vertices of influence. Figure 3.1 lights up the three vertices that are associated with the top quark. Since $W^\pm$ is a superposition of W^1 and W^2 and γ is a superposition of W^3 and B, because of the electroweak interaction, $\mathcal{O}_{tW}$ impacts all three vertices and $\mathcal{O}_{tB}$ impacts only the $t\gamma$ vertex.

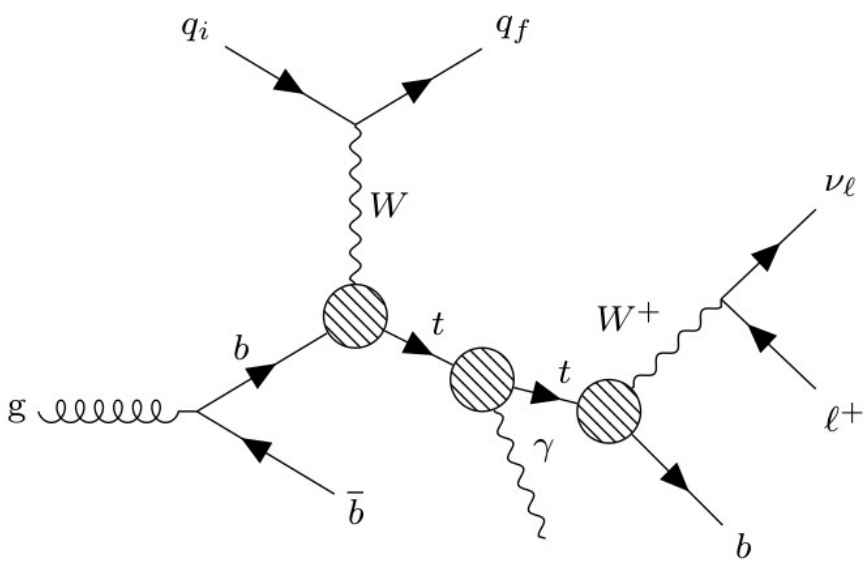

Figure 3.1: The $tq\gamma$ process with EFT affected top quark vertices marked and q_i as initial and q_f as final state hard scattering quark

4 Monte Carlo samples & event selection

This chapter examines the processes considered for the sensitivity studies of $tq\gamma$ on EFT contributions and explicates how these processes are simulated. Therefore, relevant background processes are discussed and the steps of signal and background sample generation are described. Furthermore an event selection is applied to target the suppression of non $tq\gamma$ processes.

4.1 Discussion of relevant background processes

This thesis focuses on the study of EFT contributions to $tq\gamma$ and further aims for the discrimination of SM and EFT contributions. Therefore all EFT contributions ($C \neq 0$) of the signal process $tq\gamma$ are considered as signal, whereas all SM contributions($C = 0$) are treated as background. Furthermore, all processes that can imitate $tq\gamma$ are as well treated as background. Those processes can be divided into two categories, such featuring a photon and such with misidentified photons. Background processes with a genuine photon are e.g. top quark pair production in association with a photon, where one top quark decays into a W boson that decays further into two leptons and the other decays into a W boson that decays into two quarks, or $V\gamma + jets$ production, with $V \in W^{\pm}, Z^0$. Moreover, processes that can feature a misidentified photon are $t\bar{t}$ and $V + jets$, with $V \in W^{\pm}, Z^0$ [1]. The second category is difficult to model, therefore this thesis focuses on genuine photon processes. Since the inclusion of all relevant background processes is beyond the scope of this thesis, one of the main background $t\bar{t}\gamma$ is considered.

4.2 Generation of Monte Carlo samples

The first step for the generation of Monte Carlo samples is done with MadGraph5_aMC@NLO [3], referred to as MG5. The MG6 is a matrix element event generator, which recieves an UFO [18] model as input.It is capable to model particle interactions according to the rules given by the chosen UFO model, by calculating the corresponding matrix element. Furthermore, it illustrates all feynman diagrams that are considered for this calculation. Moreover, the total cross section of the process can be evaluated. All background samples are generated according to the SM at leading order (LO) accuracy in quantum chromo dynamics, where EFT samples are generated by using DIM6Top_LO_UFO [19], referred to as DIM6TOP. It introduces dimension-six operators that are associated with top quark vertices. The DIM6TOP model uses $\mathcal{O}_{tZ}$ and C_{tZ}, which are connected to $\mathcal{O}_{tB}$ and C_{tB} by Equation 3.5 and Equation 3.6. A variation of C_{tZ} can be identified with C_{tB} via Equation 4.1, since $C_{tW} = 0$ if $C_{tZ} \neq 0$.

$$C_{tZ} = -\sin(\theta_W)C_{tB} + \cos(\theta_W)C_{tW} \tag{4.1}$$

Furthermore, all results of the thesis are presented in terms of C_{tB}. Therefore Equation 4.1 is used for this transformation.

The sample generation simulates proton proton collisions at the LHC [6] at $\sqrt{s} = 13$ TeV and applies cuts on the kinematic variables in order to lose less events because of the detector acceptance. These cuts are set to typical values describing proton proton collisions at the LHC [6]. Due to the typical coverage of detector area [20] leptons and photons are required to have a pseudorapidity $|\eta|$ smaller than five. A photon is required to have a transverse momentum of $p_T > 10$ GeV, which is perpendicular to the collision axis. Moreover an isolation criteria is applied to the angular separation of photons to quarks and leptons has to be greater than $\Delta R = \sqrt{(\Delta\eta)^2 + (\Delta\Phi)^2} = 0.2$, where $\Delta\eta$ is the difference in pseudorapidity and $\Delta\Phi$ the difference in the azimuthal angle. In addition further adjustments have been set. The parton density function NNPDF3.0NLO for 5FS is used for the $t\bar{t}\gamma$ process and the parton density function NNPDF3.0NLO for 4FS within Les Houches Accord PDF (LHAPDF) is applied for all $tq\gamma$ processes [21]. Herein 5FS corresponds to the five flavor scheme, 4FS to the four flavor scheme and LHAPDF is used as a general interface. The top quark mass is set to $m_t = 172.5$ GeV and the physical coupling constants of the electromagnetic, the Fermi and strong interaction are set to $\alpha_{\text{em}}^{-1} = 132.3489$, $G_{\text{F}} = 1.16637 \times 10^{-5}$ and $\alpha_{\text{strong}} = 1.184 \times 10^{-1}$ respectively.

The MG5 generator simulates only the hard-scattering process, but initial- and final state particles are as well exposed to strong interactions, which radiate color charged particles, that can radiate further color charged particles themselves. This phenomenon is called a parton shower. As color charged particles cannot be observed as free particles they undergo the parton shower process until they form bound states called hadrons, this process is referred to as hadronisation. Since many hadrons are formed during the process of hadronisation bundles of hadrons are formed, orientated in the same direction. These bundles of hadrons are referred to as jets. Additionally, photon emission in inital and final state as well as underlying interactions of the initial proton proton collisions, such as multiple interactions of proton compounds occur. All the stated phenomenons above are simulated by the PYTHIA8 framework [22].

Furthermore, DELPHES [23] is used as a fast detector simulation which simulates the detector response of the final particles simulated by PYTHIA8. The DELPHES simulation aims at reconstruction of events and therefore, features parametric functionsthat are used to convert the particles that reach the detector volume into physical objects, that are reconstructed from the detector response. Those

physical objects consist of leptons and photons as well as jets. For that, the detector simulation parametrization of the CMS detector [8] is used. In DELPHES FastJet [24] with the anti-k_t clustering algorithm [25] is applied for jet clustering with the radius parameter set to $\Delta R = 0.5$. Such jets are characterized by the initial particle, whereas it is difficult to reconstruct those initial particle. Because bottom quarks form B hadrons which feature a characteristic lifetime, it is possible to investigate those using the second decay vertex. Since the top quark decays very likely into a bottom quark it is important to identify those jets originating from bottom quarks, this is referred to as b-tagging. The b-tagging algorithms features the area of $|\eta| < 2.5$. Moreover neutrinos do not interact with the detector components and therefore are undetected. Since the initial particles only have an orthogonal momentum component in reference to the transverse plain of the detector, the sum of all transverse momenta $\sum_i p_T^i$ has to be zero. Hence, a sum of transverse momenta different from zero $\sum_i p_T^i \neq 0 = p_T^{miss}$ leads to a neutrino in the process.

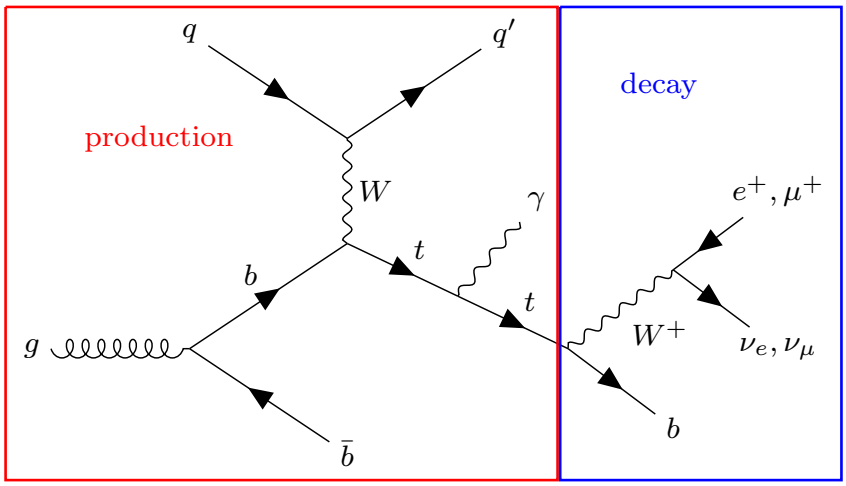

Figure 4.1: The division of the $tq\gamma$ Feynman diagram into production mode and decay mode

Furthermore the whole $tq\gamma$ process described above is split into two categories as shown in Figure 4.1, named decay mode and production mode. The production mode includes all diagrams, where a photon is radiated from one of the charged particles, which participate in the top quark production. The decay mode features all diagrams, where the photon is emitted by one of the decay products of the top quark. Samples are generated for decay, production and inclusive, production plus decay, SM contributions. Also three samples are generated including EFT effects, therefore, exhibiting non zero Wilson coefficients. Two of those model the EFT contribution and the interference term of SM and EFT contribution. The third

sample represents the former two contributions and the SM sample. The pure EFT sample and the interference sample are generated for inclusive mode of $tq\gamma$ for $C_{tW} = 2$ and $C_{tB} = 5$. The third sample, including EFT, interference and SM contributions, is generated separately for production and decay mode and each for $C_{tW} = 2$ and $C_{tB} = 5$. Additionally, a $t\bar{t}\gamma$ sample was given for this study. All samples mentioned above consist of $1,000,000$ events each and are normalized to the Run-2 integrated luminosity of the LHC of $\mathcal{L} = 139$ fb^{-1} [26]. Besides, the samples are normalized to their cross section that are listed for background samples in Table 4.1 and for signal samples in Table 4.2 and 4.3.

Table 4.1: Cross sections of generated background events

$\sigma_{\mathrm{SM,inc}}$/pb	$\sigma_{\mathrm{SM,dec}}$/pb	$\sigma_{\mathrm{SM,prod}}$/pb	$\sigma_{\mathrm{t\bar{t}}}$/pb
1.40	0.52	0.88	6.39

Table 4.2: Cross sections of generated events that feature all three contributions

$\sigma_{\mathrm{CTW,dec}}$/pb	$\sigma_{\mathrm{CTB,dec}}$/pb	$\sigma_{\mathrm{CTW,prod}}$/pb	$\sigma_{\mathrm{CTB,prod}}$/pb
0.71	0.52	1.05	0.97

Table 4.3: Cross sections of generated events that feature one of the three signal contributions

$\sigma_{\mathrm{EFT,CTB}}$/pb	$\sigma_{\mathrm{EFT,CTW}}$/pb	$\sigma_{\mathrm{INT,CTB}}$/pb	$\sigma_{\mathrm{INT,CTW}}$/pb
0.09	0.23	0.01	0.52

Furthermore small samples of $2,000$ events are generated with separately varied Wilson coefficients in the range of -4 to 4, in steps of 0.5. Those are also normalized in the same manner.

4.3 Event selection

The event selection is tailored to the $tq\gamma$ process and aims for a high efficiency for $tq\gamma$ events while reducing background contributions as much as possible. Because of that cuts on kinematic properties of physical objects are applied to the samples. First of all missing transverse energy of larger than 30 GeV is required, which is

associated with the neutrino in order to suppress background that has no genuine neutrino. Secondly, at least two jets with transverse momentum larger than 25 GeV are required. One of them needs to pass the b-tagging algorithm and an additional is required to be in the forward region, referring to a pseudorapidity of $|\eta| > 2.5$, which targets the light quark jet q' 4.1 created in the hard-scattering process with the bottom quark. Next, one photon is required with transverse momentum of at least $p_T = 15$ GeV and a pseudorapidity of $|\eta| < 2.37$. Exactly one lepton is required to fit a pseudorapidity threshold of $|\eta| < 2.5$. If the lepton is a muon it is further required to fit the transverse momentum of $p_T^{\mu} > 27$ GeV, which is a typical cut for lepton transverse momenta. The number of events after the event selection is applied is displayed for background processes in Tabular 4.4 and for signal processes in Table 4.5 and 4.6.

Table 4.4: Quantity of generated background events

$N_{SM,dec}$	$N_{SM,prod}$	$N_{t\bar{t}\gamma}$
2828	13143	57927

Table 4.5: Quantity of generated events that feature all three contributions

$N_{CTW,dec}$	$N_{CTB,dec}$	$N_{CTW,prod}$	$N_{CTB,prod}$
3467	2593	15898	16305

Table 4.6: Quantity of generated events that feature one of the three signal contributions

$N_{EFT,CTB}$	$N_{EFT,CTW}$	$N_{INT,CTB}$	$N_{INT,CTW}$
3606	4289	181	5486

5 Analysis of the Effective Field Theory sensitivity

The analysis of the $tq\gamma$ sensitivity to EFT contributions takes different steps to perform a discrimination on EFT contributions in the end. First a study of the interference of decay and production is performed. Subsequently, the impact of the Wilson coefficients on SM contributions is investigated to analyze the differences of EFT influenced samples of decay and production. Furthermore specific kinematic properties are analyzed to examine the impact of EFT contributions in comparison to the SM contributions. Finally, the discrimination of EFT and SM contributions is investigated by using a neural network approach.

5.1 Study of interference effects between production and decay contributions

To study the discrimination of EFT and SM it is helpful to first study the process itself. Due to the division of the inclusive process into production and decay as illustrated in Figure 4.1, this analysis part focuses on the differences between production and decay. Therefore, it is important to consider the possibility that both separate subregions of the inclusive process may interfere with each other. If both subprocesses do not interfere with each other, decay and production can used separately. Besides the summation of the cross sections $\sigma_{SM,inc} = \sigma_{SM,prod} + \sigma_{SM,dec}$ points towards a small interference term cross section. To investigate the interference, the transverse momentum of the photon p_T^γ is examined for production and decay individually as well as for the sum of both distributions. Additionally the p_T^γ distribution of the inclusive SM sample is shown in Figure 5.1 as interference effects would impact the distribution of this sample.

The interference plot shows that the sum of production and decay fits the inclusive distribution well within the uncertainties of both curves. This observation leads to the interpretation that no interference effects can be found. Hence, both contributions can be investigated separately. Furthermore, the interference plot shows that the production sample contributes more events to the p_T^γ plot. Also it shows a harder spectrum faster decreasing contribution.

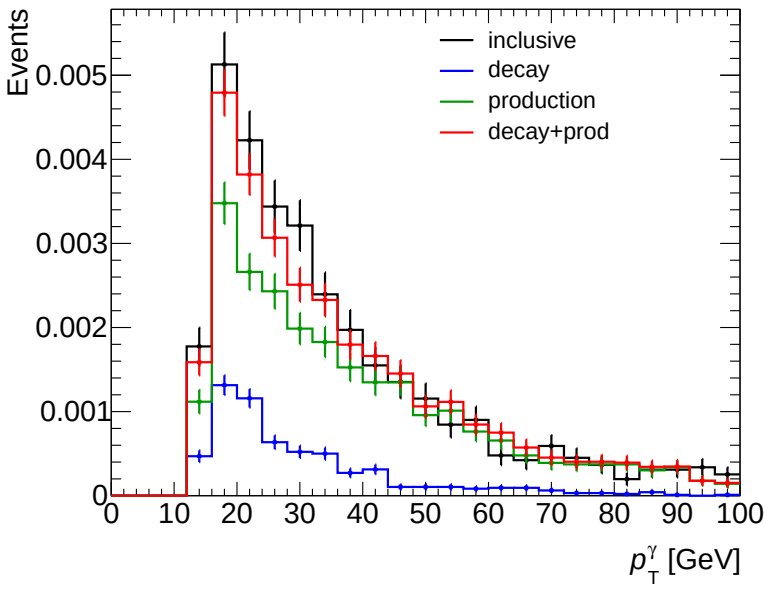

Figure 5.1: The p_T^γ spectrum of inclusive, decay and production contributions after the event selection was applied.

5.2 Dependence of the cross section on the Wilson coefficients

To retrieve a first impression of the sensitivity of $tq\gamma$ to $\mathcal{O}_{tW}$ and $\mathcal{O}_{tB}$ is inevitable to analyze the impact of the Wilson coefficients. Those Wilson coefficients directly impact the cross section of the processes. Equation 3.4 shows that the cross section depends quadratically on the Wilson coefficients. Therefore a parable shape is expected, if EFT contributions are included, and the y-intercept is expected to be the SM cross section. Figure 5.2 shows the dependence of the cross section on C_{tB} ad C_{tW} for the inclusive, production and decay contributions. In the first line the inclusive cross section is investigated, in the second the decay cross section is illustrated and in the third the production cross section is shown. A quadratic fit is applied to check the agreement of data and expectation. All six plots show good agreement to the quadratic fit, of which the $C_{tW,dec}$ and $C_{tW,prod}$ distributions fit very well. Moreover the consistency check is fulfilled for all six Figures. The inclusive C_{tB} illustration shows apparently high uncertainties for $C_{tB} = 0.5, 1, 1.5$. Statistical origins are investigated and no reason for these high uncertainties is found. All three photon origins show higher cross section values for C_{tW} than for C_{tB}, because of the number of vertices that is impacted by each operator. The decay sample

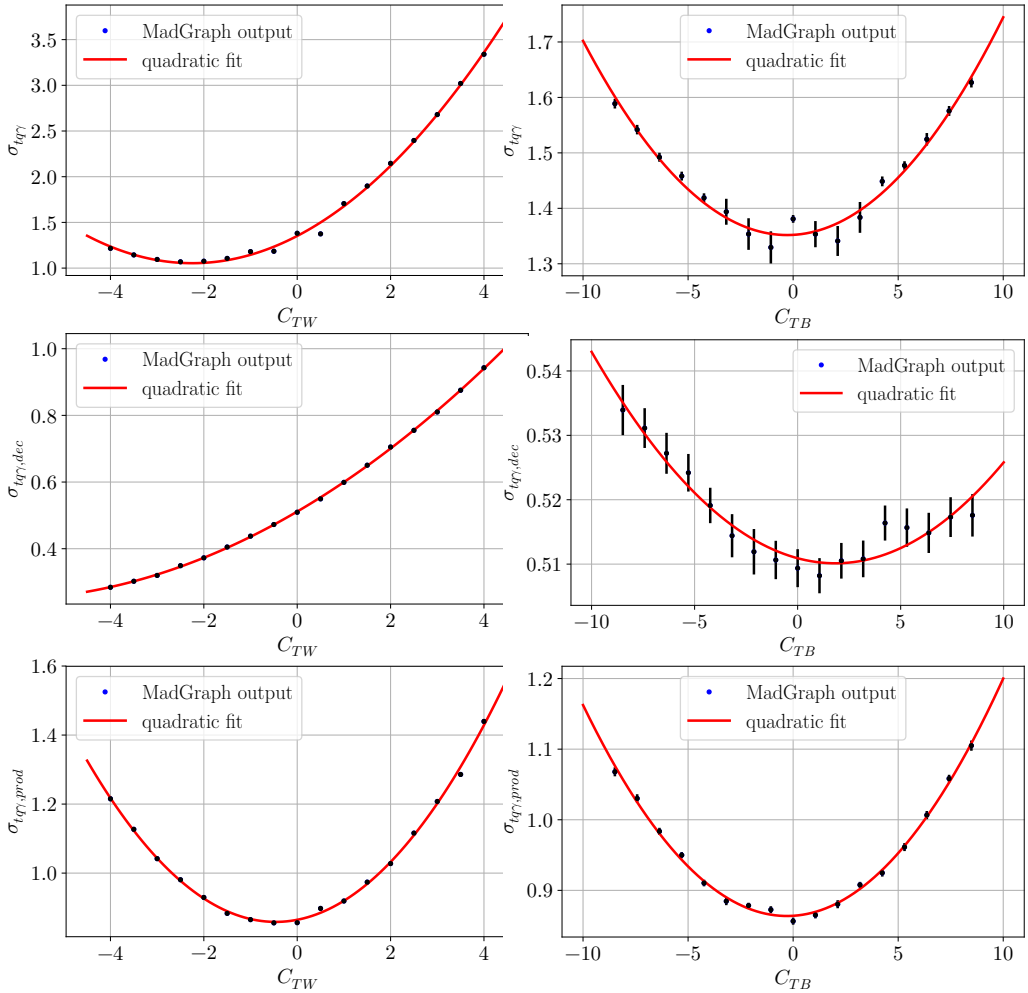

Figure 5.2: The impact of EFT operators, related to C_{tB} and C_{tW}, on the cross sections of inclusive, prodiction and decay mode

shows a way smaller sensitivity on C_{tB} in comparison to the production sample, because of its smaller range of $\sigma_{EFT} + \sigma_{int}$ in the $C_{tB,dec}$ distribution. This leads to the assumption that in the decay mode the top quark rarely emits the photon. In contrast to that show decay and production both sensitivity to C_{tW} to the same degree, due to the tW vertex in decay and production mode.

5.3 Comparison of kinematic properties of Standard Model and Effective Field Theory contributions

Kinematic properties are analyzed for the subprocesses of production and decay in order to gain further insights on the EFT contributions for both photon origins. Three kinematic properties are analyzed on the highest energetic lepton and photon in the event, namely the angular distance between lepton and photon $\Delta R(l, \gamma)$, the invariant mass of lepton and photon $m_{l\gamma}$ and the transverse momentum of the p_T^{γ}. The illustrations in Figure 5.3 consist of three histograms and a ratio plot underneath. The three histograms display the C_{tB}, the C_{tW} and the SM contribution of the corresponding photon origin, either production or decay mode. The production mode is illustrated in the first row and the decay mode in the second row. The ratio features two lines which display the ratio of the corresponding cross section to the SM cross section. Moreover it features colored points that display the event quantity ratio of EFT amd SM contributions for the specific bin. The C_{tB} contributions are pictured in green and the C_{tW} contributions are pictured in blue, while SM contributions feature red. All three decay distributions show bin depending event quantity ratios that are arranged around the cross section ratio line. This leads to the assumption that the $t\gamma$ coupling does not influence the number of events significantly. Since its change in the coupling strength should influence the shape of the distribution it is assumed that the photon is rarely emitted by the top quark in the decay. Furthermore the C_{tW} show normalization effects, since the cross section ratio is significantly higher than one. This can be interpreted as the impact of the $\mathcal{O}_{tW}$ operator on W^1 and W^2, thus also on the tW vertex.

The production mode distributions show oppositional behavior corresponding to the photon radiation of the top quark. The ratio of the $\Delta R(l, \gamma)$ illustration shows event number ratios around $\Delta R(l, \gamma) = 3$ or 4 that are higher than its cross section ratio. Also the histogram bins show a higher event output. This is indication for shape effects in the production mode The $m_{l,\gamma}$ histogram shows the increasing event ratios more clearly at higher values and strongly indicates the shape effects of C_{tW} and C_{tB} on the production mode. Additionally the last bin of the $m_{l,\gamma}$ distribution shows a higher C_{tB} event ratio value than the C_{tW} event ratio. This may seem as if

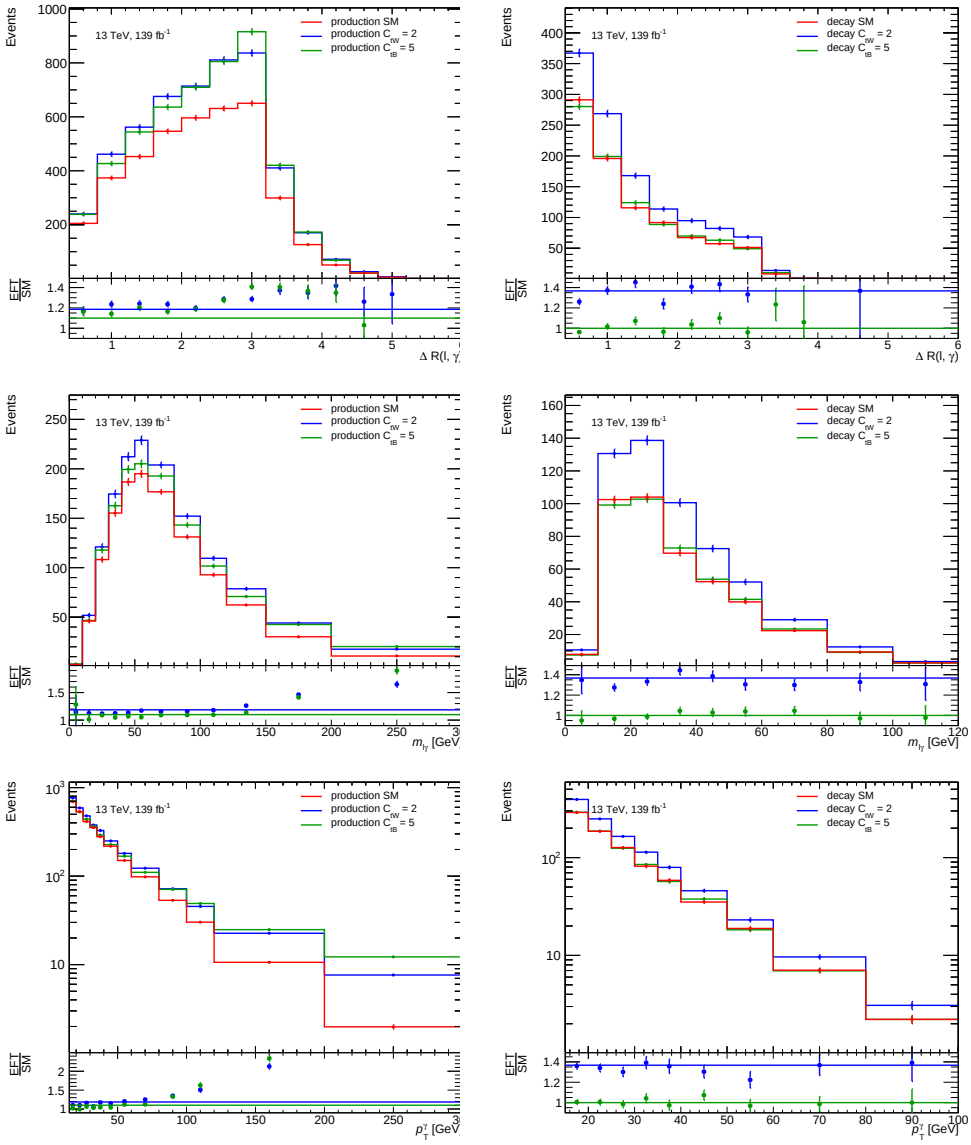

Figure 5.3: The impact of $C_{tW} = 2$ and $C_{tB} = 5$ on kinematic properties related to the photon

C_{tB} shows the stronger shape effects, but since an unequal comparison is apllied this has to be investigated further, with equal values for both Wilson coefficients. Finally the p_T^γ distribution shows a ratio higher than two for the last two bins for both distributions. Also the histogram shows a huge increase on the event ratio of EFT and SM contributions in high p_T^γ bins. Therefore shape effects are present in the production mode, but the decay mode is heavily dominated by normalization effects and no significant shape effects as well as no sensitivity on photon properties can be determined.

5.4 Discrimination of Effective Field Theory and Standard Model contributions using a neural network

The discrimination of EFT and SM contributions is the main goal of this thesis. A deep neural network is applied to accomplish the discrimination, referred to as NN. Since the decay samples do not show any sensitivity on photon properties, the approach of discriminating SM and EFT contributions on production and decay modes is discarded. Hence, an pure EFT, corresponding to $C \neq 0$, against SM ($C = 0$) approach on inclusive samples is performed. The NN study is performed separately for C_{tW} and C_{tB} and hence, two NN are set up. Herein the pure EFT events and the interference sample are treated as signal the inclusive SM sample, compound of the decay and production mode SM contributions, and the $t\bar{t}\gamma$ sample are treated as background. To make sure that the NN considers signal and background equally the normalization of the background is adjusted to the signal. The input variables given to the NN consist of p_T^γ, $|\eta_\gamma|$, Φ_γ, E_γ, p_T^l, $|\eta_l|$, Φ_l, E_l, $type_l$, p_T^{jet}, $|\eta_{jet}|$, Φ_{jet}, E_{jet}, $b-tag_{jet}$, E_T^{miss} and Φ_{miss}. Herein l describes the lepton, p_T the transverse momentum, $|\eta|$ the pseudorapidity, Φ the azimuthal angle and E the energy. A benchmark NN scenario is applied and since this targeted discrimination is a binary classification problem, a Deep Neural Network approach is used. The structure of the NN is illustrated in Tabular 5.1. five layers of which five are fully connected dense layers. On the first layer the input shape equals the number of input variables of the training set. The total number of parameters used in this specific NN is 1078 and all of these are trainable.

The activation function between the dense layers is chosen to be a Leaky Rectified Linear Unit (ReLU) function. It is defined by Equation 5.1.

$$f(x) = \begin{cases} 0.05\ \mathrm{x} & \text{for} \quad \mathrm{x}<0 \\ \mathrm{x} \quad \text{for} \quad \mathrm{x}\ 0 \end{cases} \tag{5.1}$$

Table 5.1: The structure of the applied deep neural network

Layer	Number of nodes	Number of trainable parameters
Dense layer 1	17	289
Dense layer 2	24	432
Dense layer 3	12	300
Dense layer 4	4	52
Dense layer 5	1	5

The activation function of the output layer used in this NN is the sigmoid function and it is defined by Equation 5.2.

$$sigmoid(x) = \frac{e^x}{1 + e^x} \tag{5.2}$$

Its codomain is ranged between zero and one, where zero is assigned to events that are classified as backgrounds and one is assigned to these that are classified as signal. The defined loss function is the binary cross entropy shown in Equation 5.3, where $f()$ is the sigmoid function and s_i and t_i are the score and the gorundtruth of signal or background. The metric that is used to evaluate the performance of the classification of this NN is the accuracy between signal and background shown in Equation 5.4, where C stands for the sum of the correct distributed events of signal and background and F stands for the incorrect distributed events.

$$Loss = -\sum_{i=1}^{2} t_i log(f(s_i)) \tag{5.3}$$

$$Accuracy = \frac{C}{C + F} \tag{5.4}$$

Besides the chosen optimization algorithm is the Adam optimizer [27]. The full sets of signal and background events are split into training, validation and test set, where the respective set sizes are

63.75% training data,
25% validation data,
11.25% testing data,

with respect for the complete data set. The NN is trained with a batch size of 100, therefore bunches of 100 events each are used to train the NN. After all events were used once in the training of the NN it has been trained one epoch. The NN is trained 150 epochs.

First, the NN output is described for the discrimination of SM and EFT contributions with $C_{tW} = 2$, second for $C_{tB} = 5$. Figure **??** displays the accuracy of the NN in dependence of the trained epochs.

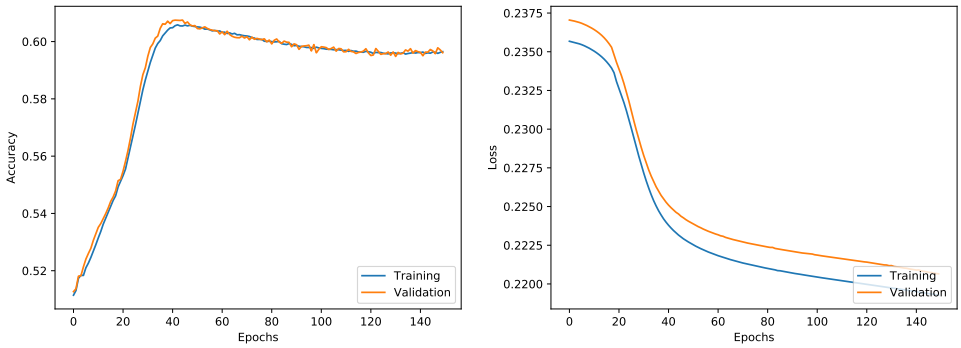

Figure 5.4: The NN accuracy and loss for the NN trained on the C_{tW} data set.

Figure 5.4 illustrates the loss of the NN. The blue graph describes the performance on the training set. As the loss curve decreases the NN learns about the discrimination of the data in the training and in the validation data. Furthermore, the training and validation curve differ only slightly in value and due to the offset of both curves which does not increase in the last epochs no signs of overtraining are observed. Both curves reach a loss value of 0.22. The accuracy increases for the first epochs then it slightly decreases and then converges towards 59%. The validation graph in orange mainly mimics the training graph. It fluctuates for the last epochs around the training accuracy and similarly reaches a final accuracy of 59%.

Moreover, the trained NN is evaluated on the test dataset as well as on the validation and training dataset, to validate the structure of the NN and to check whether overtraining can be found. Figure 5.5 shows the binned NN-output of all three datasets normalized to the unit area. The signal distributions all three exhibit nearly the same shape and find their distribution orientated towards one. Also the shapes of the background datasets show only tiny discrepancies, but orientate stronger towards an output of zero. As signal and background distributions significantly overlap and are centered around 0.5, the NN does not separate these samples fully. Due to the tiny discrepancies no overfitting is observed and and the NN is validated. Finally the NN is evaluated on the datasets of $t\bar{t}\gamma$, $tq\gamma_{dec}$, $tq\gamma_{prod}$, $tq\gamma_{CTW,INT}$ and $tq\gamma_{CTW,EFT}$. The stacked NN output is shown in Figure 5.5. The $t\bar{t}\gamma$ process dominates this distribution, due to its six times higher cross section. Besides the 1.0 bin is mainly filled with pure EFT and interference samples. Furthermore, the ratio

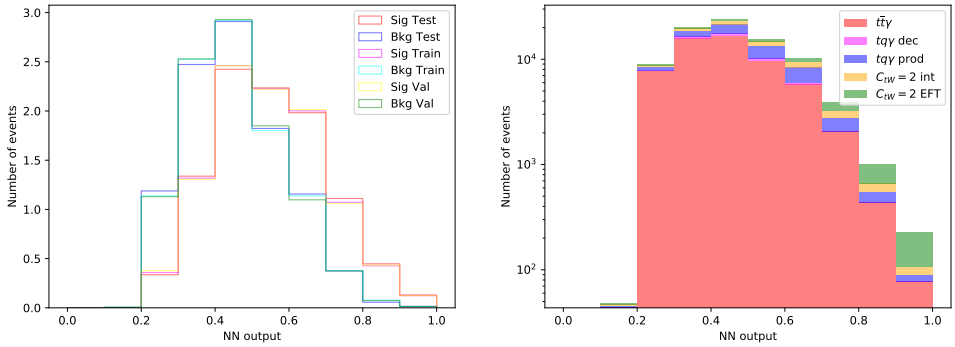

Figure 5.5: On the left the discrimination of train, test and validation data set and on the right the NN output for the discrimination of different signal and background samples. The Signal EFT contributions correspond to C_{tW} and all distributions are normalized to unit area

of signal and background distributions increase for higher NN outputs. This leads to the deduction that the NN is able to separate the samples towards the right values. Hence the NN is able to provide discrimination of EFT and SM contributions.

Second, the NN is trained for $C_{tB} = 5$. For that also binary accuracy and binary cross entropy are illustrated in Figure 5.6. The accuracy shows continuously increasing

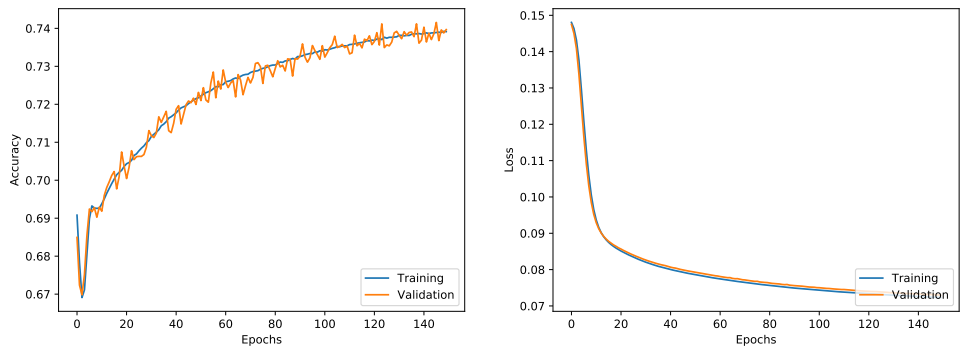

H

Figure 5.6: The NN accuracy and loss for the NN trained on the C_{tB} data set.

progress through all 150 epochs of training, except for random fluctuations of the initial NN parameters in the first two epochs. The validation data set matches the training curve but fluctuates around the training accuracy, because of its smaller size. For the last epochs the NN converges to an accuracy of 74% for both datasets. The

loss curve shows a steeply decreasing loss for the first epochs, which indicates that the discrimination power of the NN steeply rises. Furthermore, the loss decreases till the end of the training. The difference between validation and training loss are very small and both reach a loss of 0.07. Concluding, the NN is evaluated with the test, validation and training datasets. The NN outputs for the three datasets are illustrated in Figure 5.7, for signal and background separately and the distributions are normalized to unit area.

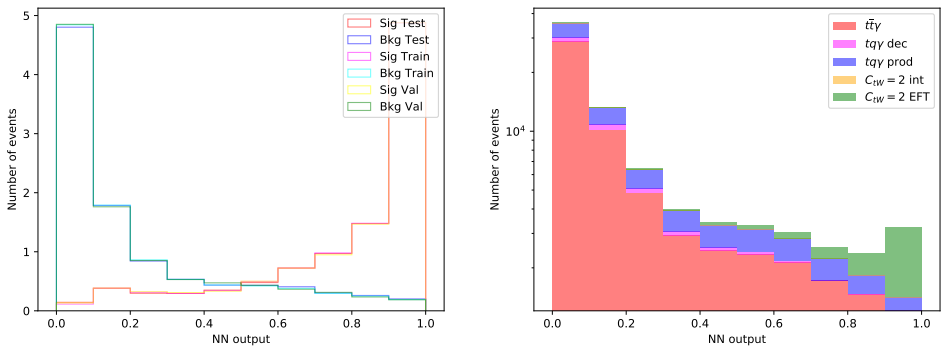

Figure 5.7: On the left the NN output of signal and background events for train, test and validation dataset and on the right the discrimination of background and signal events. The Signal EFT contributions correspond to C_{tB} and all distributions are normalized to unit area

The NN separates the signal and background contributions very well and only a small overlap can be seen. Besides, the NN also provides a strong separation of signal and background events, as the number of events increase and decrease monotonously towards one and zero. Finally, the NN is evaluated on different processes separately [**fig:fig17**]. Herein $t\bar{t}\gamma$ also dominates the distribution but EFT samples are clearly separated towards the signal-like values. Therefore, it can be conluded that the NN does discriminate EFT contributions very good from SM events.

6 Conclusions

The sensitivity of the single top production with a photon on EFT operators $\mathcal{O}_{tW}$ and $\mathcal{O}_{tB}$ has been investigated and an analysis on the discrimination of EFT and SM contributions has been performed. For that, all EFT contributions to $tq\gamma$ have been treated as signal, where SM $tq\gamma$ and $t\bar{t}\gamma$ have been treated as backgrounds. The process has been subdivided into events where the photon is emitted in the production of the top quark, referred to as production mode and those where the photon is radiated in the decay of the top quark, referred to as decay mode. Furthermore MC samples have been produced for the contributions that arise purely from EFT, from the interference of SM and EFT and purely for SM as well as one sample covering all contributions, referred to as total EFT. A total EFT sample and a SM sample have been generated for production and decay mode each. An event selection has been applied to suppress non $tq\gamma$ processes. Moreover, interference studies of production and decay mode samples have been performed and no interference has been observed. Therefore production and decay mode can be investigated separately.
The EFT operators $\mathcal{O}_{tW}$ and $\mathcal{O}_{tB}$ have been described and the sensitivity of decay and production modes on those operators has been investigated. First of all, the impact of the operators on the cross sections has been evaluated. The production mode features sensitivity to $\mathcal{O}_{tW}$ and $\mathcal{O}_{tB}$, where the decay mode is characterized by sensitivity to $\mathcal{O}_{tW}$, but only very small sensitivity to $\mathcal{O}_{tB}$, which indicates that the photon is rarely emitted from the top quark in the decay mode. Furthermore, photon related kinematic variables have been examined in order to evaluate whether the EFT operators impact the shape of those variables. For the $\mathcal{O}_{tW}$ and $\mathcal{O}_{tB}$ impact on the production mode significant shape impacts are observed. No such shape effects have been observed for the decay mode.

Therefore it is concluded that the sensitivity on EFT contributions does not benefit from the separate analyzing of EFT contribution to production and decay mode.
Thus, the discrimination of inclusive SM samples and EFT contributions is performed by setting up a NN. Two identical NN have been trained with SM contributions as background and EFT contributions as signal separately for $C_{tW} = 2$ and $C_{tB} = 5$ contributions. The NN output features good accuracy values for $C_{tW} = 2$ and shows a good discrimination due to the high signal background ratio for high output values. For the C_{tB} training, the NN reaches high accuracy values and high power of discrimination can be found because of the strongly increasing signal background ratios for high NN output values. Hence the NN is able to separate EFT from SM contributions and therefore future studies based on the achievements of this thesis feature very high potential to further increase the knowledge of the EFT influenced process. Moreover, studies on the optimization of the NN may lead to even better discrimination and further expansion of these studies will increase the understanding of the impact of the EFT operators on the $tq\gamma$ process.

Literatur

[1] CMS Collaboration, "Evidence for the associated production of a single top quark and a photon in proton-proton collisions at $\sqrt{s} = 13TeV$", Phys.Rev.Lett. **121** (2018) S. 221802.

[2] Jan Lukas Späh, "Studies for the sensitivity to dimension six operators in the context of the effective field theories in single-top-quark production with a photon", (2019).

[3] J. Alwall et al., "The automated computation of tree-level and next-to-leading order differential cross sections, and their matching to parton shower simulations", Journal of High Energy Physics **2014** (2014).

[4] ATLAS collaboration, "The Standard Model and beyond", (2020), URL: `http://united-states.cern/physics/standard-model-and-beyond`.

[5] ATLAS Collaboration, "Measurement of the top-quark decay width in top-quark pair events in the dilepton channel at $\sqrt{s} = 13$ TeV with the ATLAS detector", (2019).

[6] Lyndon Evans und Philip Bryant, "LHC Machine", Journal of Instrumentation **3** (2008) S08001.

[7] Tevatron Electroweak Working Group, "Combination of CDF and D0 Measurements of the Single Top Production Cross Section", (2009), arXiv: `0908.2171 [hep-ex]`.

[8] CMS Collaboration, "The CMS Experiment at the CERN LHC", JINST (2008) S08004.

[9] "Matter and antimatter in the universe", New Journal of Physics (2012) S. 095012, hrsg. von M. Drewes L. Canetti und M. Shaposhnikov.

[10] F. Zwicky, "Die Rotverschiebung von extragalaktischen Nebeln", Helv. Phys. (1933) S. 110.

[11] Y. et al. Fukuda, "Evidence for Oscillation of Atmospheric Neutrinos", Physical Review Letters **81** (1998) S. 1562.

[12] Jianlong Lu, "Why Neutrino Masses Cannot Arise from Nonzero VEV of Charged Higgs Field in the Only Higgs Doublet", (2020), arXiv: `2005.00390 [hep-ph]`.

[13] KATRIN Collaboration, "Improved Upper Limit on the Neutrino Mass from a Direct Kinematic Method by KATRIN", Phys. Rev. Lett. **123** (2019) S. 221802.

[14] Gia Dvali und Glennys R. Farrar, "Strong CP Problem with 10^{32} Standard Model Copies", Physical Review Letters **101** (2008).

[15] M. et al. Aaboud, "Measurement of the W-boson mass in pp collisions at

$$\sqrt{s} = 7\,TeV$$

with the ATLAS detector", The European Physical Journal C **78** (2018).

[16] A. et al. Barczyk, "Measurement of the Fermi constant by FAST", Physics Letters B **663** (2008) S. 172.

[17] E. Fermi, "Versuch einer Theorie der β-Strahlen", Z.Phys. **188** (1934) S. 161.

[18] Céline Degrande et al., "UFO – The Universal FeynRules Output", Computer Physics Communications **183** (2012) S. 1201.

[19] "The DIM6Top_LO_UFO model", (2020), URL: `https://feynrules.irmp.ucl.ac.be/wiki/dim6top`.

[20] "The ATLAS Experiment at the CERN Large Hadron Collider", JINST (2008) S08003, hrsg. von ATLAS Collaboration.

[21] Ball et al., "Parton distributions for the LHC run II", Journal of High Energy Physics **2015** (2015).

[22] Sjöstrand et al., "An introduction to PYTHIA 8.2", Computer Physics Communications **191** (2015) S. 159.

[23] S. Ovyn, X. Rouby und V. Lemaitre, "Delphes, a framework for fast simulation of a generic collider experiment", (2009), arXiv: `0903.2225 [hep-ph]`.

[24] G. P. Salam M. Cacciari und G. Soyez, "FastJet User Manual", Eur. Phys. J. C **72** (2012) S. 1896, arXiv: `1111.6097 [hep-ph]`.

[25] G. P. Salam M. Cacciari und G. Soyez, "The anti-k_t jet clustering algorithm", JHEP **04** (2008) S. 063, arXiv: `0802.1189 [hep-ph]`.

[26] ATLAS Collaboration, "Luminosity determination in *pp* collisions at $\sqrt{s} = 13$ TeV using the ATLAS detector at the LHC", (2019).

[27] Diederik P. Kingma und Jimmy Ba, "Adam: A Method for Stochastic Optimization", (2014), arXiv: `1412.6980 [cs.LG]`.

Danksagung

Zunächst bedanke ich mich bei Herrn Priv.-Doz. Dr. Johannes Erdmann, der es mir ermöglicht hat und mich motiviert hat, die vorliegende Bachelorarbeit am Lehrstuhl für Experimentelle Physik IV in Dortmund zu schreiben. Außerdem danke ich Ihm für die freundliche und hilfreiche Betreuung im Rahmen von Gesprächen und Anregungen, sowie für die Erstkorrektur dieser Arbeit. Weiterhin danke ich Herrn Prof. Dr. Bernhard Spaan für die Zweitkorrektur der vorliegenden Arbeit. Ich danke Herrn Prof. Dr. Kevin Kröninger, dass es mir ermöglicht wurde diese Arbeit am Lehrstuhl Experimentelle Physik IV zu schreiben. Außerdem danke ich ausgiebig Herrn Björn Wendland für die mehr als freundliche, freundschaftliche Betreuung meiner Bachelorarbeit, für jedes Gespräch und die vielen Zwischenfragen, sowie zahlreiche Korrekturen zu jeder Tageszeit. Ich danke Frau Sara Krieg die durch Ihren Einsatz und das Korrekturlesen mehrerer Kapitel beigetragen hat. Ich danke Frau Alina Joch und Herrn Tristan Gradetzke für ihre Korrekturen. Zudem danke ich allen weiteren Bachelorstudenten des Lehrstuhls für anregende und ausgiebeige Unterhaltungen. Zum Schluß danke ich meiner Familie und meinen Freunden die mich ausgiebigst bei der Ausführung dieser Arbeit unterstützt haben.

Eidesstattliche Versicherung

Ich versichere hiermit an Eides statt, dass ich die vorliegende Abschlussarbeit mit dem Titel „Discrimination of Standard Model and EFT contributions in single top production with a photon“ selbstständig und ohne unzulässige fremde Hilfe erbracht habe. Ich habe keine anderen als die angegebenen Quellen und Hilfsmittel benutzt, sowie wörtliche und sinngemäße Zitate kenntlich gemacht. Die Arbeit hat in gleicher oder ähnlicher Form noch keiner Prüfungsbehörde vorgelegen.

Dortmund, den 24.06.2020

Ort, Datum

Unterschrift

Belehrung

Wer vorsätzlich gegen eine die Täuschung über Prüfungsleistungen betreffende Regelung einer Hochschulprüfungsordnung verstößt, handelt ordnungswidrig. Die Ordnungswidrigkeit kann mit einer Geldbuße von bis zu 50 000 € geahndet werden. Zuständige Verwaltungsbehörde für die Verfolgung und Ahndung von Ordnungswidrigkeiten ist der Kanzler/die Kanzlerin der Technischen Universität Dortmund. Im Falle eines mehrfachen oder sonstigen schwerwiegenden Täuschungsversuches kann der Prüfling zudem exmatrikuliert werden (§ 63 Abs. 5 Hochschulgesetz –HG–).

Die Abgabe einer falschen Versicherung an Eides statt wird mit Freiheitsstrafe bis zu 3 Jahren oder mit Geldstrafe bestraft.

Die Technische Universität Dortmund wird ggf. elektronische Vergleichswerkzeuge (wie z. B. die Software „turnitin“) zur Überprüfung von Ordnungswidrigkeiten in Prüfungsverfahren nutzen.

Die oben stehende Belehrung habe ich zur Kenntnis genommen.

Dortmund, den 24.06.2020

Ort, Datum

Unterschrift